Magn Reson Imaging. Author manuscript; available in PMC 2010 September 22.

Published in final edited form as:

Magn Reson Imaging. 2010 June ; 28(5): 621–628. doi:10.1016/j.mri.2010.03.011.

Combined prostate Diffusion Tensor Imaging and Dynamic Contrast Enhanced MRI at 3T – quantitative correlation with biopsy

Piotr Kozlowski, PhD[1,2,3,4], **Silvia D. Chang, MD**[1,2,3], **Ran Meng**[4], **Burkhard Mädler, PhD**[4,5], **Robert Bell, MSc**[1], **Edward C. Jones, MD**[6], and **S. Larry Goldenberg, MD**[1,3]

[1] The Prostate Centre at Vancouver General Hospital, Vancouver BC, Canada

[2] University of British Columbia, Department of Radiology, Vancouver BC, Canada

[3] University of British Columbia, Department of Urologic Sciences, Vancouver BC, Canada

[4] University of British Columbia MRI Research Centre, Vancouver BC, Canada

[5] Philips Healthcare, Vancouver BC, Canada

[6] University of British Columbia, Department of Pathology and Laboratory Medicine, Vancouver BC, Canada

Abstract

The purpose of this work was to compare diagnostic accuracy of Diffusion Tensor Imaging (DTI), Dynamic Contrast Enhanced MRI (DCE MRI), and their combination in diagnosing prostate cancer. Twenty five patients with clinical suspicion of prostate cancer underwent MRI, prior to transrectal ultrasound (TRUS)-guided biopsies. MRI data were correlated to biopsy results. Logistic regression models were constructed for the DTI parameters, DCE MRI parameters, and their combination. The areas under the Receiver Operator Characteristic curves (AUC) were compared between the models. The nonparametric Wilcoxon signed rank test was used for statistical analysis. The sensitivity and specificity values were respectively 81% (74% – 87%) and 85% (79% – 90%) for DTI and 63% (55% – 70%) and 90% (85% – 94%) for DCE. The combination “DTI or DCE MRI” had 100% (97% – 100%) sensitivity and 77% (69% – 83%) specificity, while “DTI and DCE MRI” had 44% (37% – 52%) sensitivity and 98% (94% – 100%) specificity. The AUC for DTI + DCE parameters was significantly higher than that for either DTI (0.96 vs. 0.92, p = 0.0143) or DCE MRI parameters (0.96 vs. 0.87, p = 0.00187) alone. In conclusion, the combination of DTI and DCE MRI has significantly better accuracy in prostate cancer diagnosis than either technique alone.

Corresponding author: Piotr Kozlowski, Life Sciences Centre, 2350 Health Sciences Mall, Vancouver BC, Canada V6T 1Z3, tel.: (604) 827-3974, fax: (604) 827-3973, pkozlow@interchange.ubc.ca.

Part of this work has been presented at the 18th Annual Meeting of the International Society for Magnetic Resonance in Medicine, abstract #2245.

Keywords

Diffusion Tensor Imaging; Dynamic Contrast Enhanced MRI; prostate cancer; 3T; biopsy; logistic regression analysis

Introduction

Non-invasive identification and localization of prostate cancer remains challenging. MRI is arguably the best non-invasive diagnostic method available. Relatively low sensitivity and specificity of the traditionally used T_2-weighted images can be improved to some degree with other MRI techniques such as Diffusion Tensor Imaging (DTI) [1, 2], Dynamic Contrast Enhanced (DCE) MRI [3, 4] and MR Spectroscopic Imaging (MRSI) [5, 6]. Recently, a number of studies suggested that a combination of several MRI techniques can further improve the MRI capability of diagnosing prostate cancer [7–14]. Most of these techniques, however, were based on the qualitative assessment of the MRI exams by an experienced reader.

In this study we used a combination of DTI and DCE MRI with quantitative analysis, using biopsy as a reference standard, to test whether this combination improves the sensitivity and specificity over either technique alone. The presence or absence of cancer was evaluated based on the numerical values of 5 MRI parameters calculated from DTI and DCE MRI data. In addition, logistic regression modeling was used to construct a predictor that can estimate the probability of any pixel within parametric maps representing cancer.

In a previous study at 1.5T we have shown that a combination of the Diffusion Weighted (DW) and DCE MRI provides higher sensitivity in diagnosing prostate cancer than either technique alone [14]. In this study we tested whether with the expected improvement in data quality at a higher field of 3.0T, the combination of diffusion and DCE MRI remains more accurate in prostate cancer diagnosis that either of these techniques alone.

Materials and Methods

Patient selection and biopsy technique

This prospective study was approved by the institutional human ethics board, and all participants gave signed consent prior to entering the study. Twenty five patients with a high clinical suspicion for prostate adenocarcinoma due to an elevated prostate specific antigen (PSA) and/or palpable prostatic nodule, with no prior treatment, were consecutively recruited to this study. Standard MRI exclusion criteria (e.g. pacemaker, metallic implants, known allergy to MRI contrast agent, etc.) were applied during patients' selection process. Unlike in most prostate MRI studies, subjects recruited to this study underwent MRI examination prior to transrectal ultrasound (TRUS)-guided biopsies. Such recruitment process ensures that the study is truly prospective in its assessment as a diagnostic tool, and that no artifacts resulting from biopsies are present in the MRI images.

TRUS biopsies of the prostate were performed on a GE Logic 9 ultrasound machine (GE Healthcare, Milwaukee, WI). The patients were examined with gray scale imaging in the

axial and sagital planes with a 5 MHz transrectal probe. All patients had an enema and were given prophylactic antibiotics prior to performing the prostate biopsies. The biopsies were performed under local anesthetic and the number of biopsies obtained from the peripheral zone (PZ) was determined by prostate gland size. In patients with a prostate gland of 30 cc or less, eight biopsies (base: right and left; midgland: right lateral, left lateral, right medial, left medial; apex: right and left) were taken. For prostate glands ranging 31–60 cc, 10 biopsies (base: right lateral, left lateral, right medial, left medial; midgland and apex biopsies as above) were obtained. For prostate glands greater than 60 cc, 12 biopsies were obtained (apex: right lateral, left lateral, right medial, left medial, base and midgland biopsies the same as the 10 biopsy scheme).

MRI examinations

All MRI examinations were performed on a 3T MRI scanner (Achieva, Philips Healthcare, Best, the Netherlands). MRI signals were acquired with a combination of an endorectal coil (Medrad, Pittsburgh, PA, USA) and a cardiac phased-array coil (Philips Healthcare, Best, the Netherlands). Fast spin-echo T_2-weighted images (repetition time TR = 1851 ms, effective echo time TE = 80 ms, field of view FOV = 14 cm, slice thickness = 4 mm with no gap, 284×225 matrix, 3 averages) were acquired in the axial and coronal planes to provide anatomical details of the prostate. From this sequence, 12 axial slices covering the entire gland were then selected and used for the DTI and DCE MRI scans.

DTI data were acquired using a diffusion weighted single shot echo planar imaging (EPI) sequence (TR/TE = 2100/74 ms, FOV = 24 cm, slice thickness = 4 mm with no gap, 128×115 matrix, 6 non-collinear gradient directions, b-value = 0 and 600 sec/mm^2, 18 averages, total acquisition time of 8 minutes; the relatively low b-value of 600 sec/mm^2 was chosen to ensure sufficient SNR for quantitative measurements of DTI parameters).

DCE MRI was performed using a 3D T_1-weighted (T1W) spoiled gradient echo sequence (TR/TE = 3.4/1.06 ms, flip angle = 15°, FOV = 24 cm, 256×163 matrix, 2 averages). Initially, proton density (PD) images (TR/TE = 50/0.95 ms, flip angle = 4°) were acquired to allow calculation of the contrast agent concentrations in the prostate [15]. Next, a series of 75 T1W images were acquired prior to (3 images) and following (72 images) a bolus injection of Gd-DTPA (Magnevist, Berlex Canada, 0.1 mmol/kg injected with a motorized power injector within 10 s followed by a 20 ml flush of saline). This resulted in a time resolution of 10.6 sec per 12 slices. The total time of the MRI examination was approximately 45 minutes.

Data processing

The DTI data were processed off-line. Diffusion weighted images were registered to the non-weighted b=0 image with a mutual information algorithm prior to calculating the eigenvalues of the diffusion tensor and generating maps of the average diffusivity <D> (i.e. trace of the diffusion tensor) and fractional anisotropy (FA) with the proprietary DTI processing toolbox PRIDE (Philips Healthcare, Best, the Netherlands).

DCE MRI data were processed off-line with software procedures developed in house using Matlab (Mathworks, Natick, MA, USA) and Igor Pro (WaveMetrics, Portland, OR, USA).

Prior to further processing, T1W and PD images were registered to one another using PRIDE. Contrast agent concentration maps were calculated from the T1W and PD images as described in [15]. Arterial Input Functions (AIFs) were extracted from voxels in the external iliac or femoral arteries in the central slice for each patient [16]. It has been shown that even with relatively low temporal resolution of 10 seconds per time point used in this study, the patient specific AIF provides more accurate fitting in highly enhancing areas than the population average AIF [17]. Pharmacokinetic parameters: volume transfer constant – K^{trans}, fractional volume of the extra-vascular extra-cellular space – v_e, and fractional plasma volume – v_p, were calculated by fitting the contrast agent concentration vs. time curves to the extended Kety model [18]. Hematocrit value was assumed to be 0.42 [16]. Fitting was carried out in every pixel of every slice within a region of interest (ROI) encompassing the prostate gland to generate maps of the pharmacokinetic parameters.

To correlate DTI and DCE MRI parameters with biopsy results regions in the parametric maps corresponding to biopsy locations were classified as either tumor or normal PZ based on a threshold values in <D> and K^{trans} maps. It has been shown previously that in prostate tumors <D> is lower and K^{trans} is higher than in normal PZ [14, 19, 20]. Thus the threshold value for <D> was calculated as the average plus one standard deviation in ROIs manually drawn around low <D> regions in the images corresponding to the biopsy-confirmed cancer and <D> below the threshold was considered to denote cancer. Subsequently the ROIs denoting cancer on DTI data were drawn based on the <D> threshold value and average values of <D> and FA were calculated in these ROIs. Similarly, the threshold value for K^{trans} was calculated as the average minus one standard deviation in ROIs manually drawn around high K^{trans} regions in the images corresponding to biopsy-confirmed cancer, and K^{trans} above the threshold was considered to denote cancer. Again, the ROIs denoting cancer on DCE MRI data were drawn based on the K^{trans} threshold value and the average values of K^{trans}, v_e, and v_p were calculated in these ROIs. In the parametric maps where no low <D> or high K^{trans} areas were present, the average parameter values were calculated from the entire area corresponding to the biopsy location. The average values of the MRI parameters in the central gland (CG) were calculated from the ROIs encompassing entire CG within the midgland part of the prostate in patients with negative biopsies only. These values were calculated to provide comparison with the normal cancerous PZ and no distinction between benign prostatic hyperplasia (BPH) and normal CG was attempted.

Statistical analyses were carried out using JMP 4.0 (SAS Institute Inc., Cary, NC). The statistical significance of the differences between tumor, normal PZ, and normal CG was performed using the nonparametric Wilcoxon signed rank test. Sensitivity, specificity, positive predictive value (PPV), negative predictive value (NPV) and accuracy were calculated according to formulas in [21]. 95% confidence intervals were calculated using the efficient-score method corrected for continuity [22]. Receiver Operating Characteristic (ROC) curves were generated with the JMP software.

To compare the performance of the DTI and DCE MRI parameters in predicting the biopsy result, a logistic regression model was constructed using R 2.7.0 – a language and environment for statistical computing (R Foundation for Statistical Computing, Vienna, Austria, ISBN 3-900051-07-0, URL http://www.R-project.org). A leave-one-out-cross-

validation (LOOCV) was used to test the quality of the predictor resulting from the logistic regression [23]. Three models were constructed: DTI parameters only, DCE MRI parameters only, and all MRI parameters. To quantify the quality of the predictor based on each model, the ROC curves were constructed and the areas under the ROC curves (AUC) were compared, taking into account that ROC curves were correlated [24].

Results

Of the 25 men recruited to the study between March 2008 and January 2009, one patient cancelled his participation prior to the MRI exam and two patients did not complete the MRI exam due to claustrophobia. The average age of the 22 patients who completed the study was 61.7 years (38 – 72 years) and their average PSA level was 8.5 ng/mL (0.94 – 15 ng/mL). Ten of the 22 patients had biopsy confirmed prostatic adenocarcinoma with 27 positive biopsies in total. In two patients (both with negative biopsies) excessive motion precluded the accurate estimate of the AIF and thus DCE data from these patients were not included in the overall analysis. Clinical data (i.e. age, PSA levels, number of positive biopsies, biopsy and prostatectomy Gleason scores, and clinical stage) for the ten patients who had biopsy confirmed cancer are summarized in Table 1.

Figure 1a shows representative T_2 weighted images and the corresponding <D>, FA, K^{trans} and v_e maps from patients with biopsy proven adenocarcinoma (top) and negative biopsies (bottom). Average values of <D>, K^{trans} and v_p showed significant differences between tumor and normal PZ (Table 2). Figure 1b shows AIF and representative concentration vs. time curves from PCa, normal PZ, and CG.

Table 3 shows the performance measures for the DTI and DCE MRI and their combinations. DTI had higher sensitivity than DCE (81% vs. 63%), while DCE had higher specificity than DTI (90% vs. 85%). The combination “DTI or DCE” had perfect sensitivity of 100%, i.e. all biopsy confirmed cancers were detected with either technique. The highest specificity of 98% was achieved when the tumors were confirmed by both techniques. This combination “DTI and DCE” also had the highest PPV of 80% and the overall accuracy of 91%.

Out of 177 negative biopsies, 41 were identified as MRI false positives with either technique. Some of these biopsies were identified in pathology reports as high grade prostatic intraepithelial neoplasia (PIN – the precursor of prostatic adenocarcinoma), prostatitis, or suspicious but not diagnostic pathological changes. Out of 4 biopsies identified as high grade PIN, 2 had both low <D> and high K^{trans}, 1 had low <D> and normal K^{trans}, and 1 had normal values of both <D> and K^{trans}. However, out of 4 biopsies identified as prostatitis, 3 had low <D>, but none had increased K^{trans}. Thus the combination of DTI and DCE may potentially help to distinguish between prostatitis and adenocarcinoma, although more studies are needed to prove this.

Out of 27 positive biopsies 5 were false negatives on DTI. In one case a true positive was identified in the neighboring location (i.e. right mid medial core was DTI true positive, while right mid lateral core was DTI false negative), thus the false negative might have been due to possible biopsy sampling error. All remaining false negatives had <D> values lower than in

normal PZ, but higher than the threshold value. All these biopsies were identified as Gleason 3+3 adenocarcinoma.

Figure 2a shows ROC curves generated for each MRI parameter. The average diffusivity <D> had the highest area under the ROC curve (AUC) value of 0.91 among all the parameters, followed by K^{trans} (0.84) and v_p (0.76). FA and v_e had the values close to 0.5 (0.54 and 0.59 respectively), suggesting that these parameters alone are not particularly useful in distinguishing between cancer and normal PZ. This is consistent with the Wilcoxon test showing no significant difference in FA or v_e between carcinoma and normal PZ (Table 2). Logistic regression model generated the ROC curves for groups of DTI (i.e. <D> and FA) and DCE MRI (i.e. K^{trans}, v_e, and v_p) parameters (Figure 2b). The AUC calculated for DTI + DCE (i.e. <D>, FA, K^{trans}, v_e, and v_p) parameters was significantly higher than that for either the DTI parameters: 0.96 vs. 0.92, $p = 0.0143$, or the DCE MRI parameters: 0.96 vs. 0.87, $p = 0.00187$ alone.

Discussion

The results of this study demonstrate that the combination of DTI and DCE MRI techniques significantly improves the capability of either of these techniques for diagnosing prostate cancer. Indeed, all biopsy confirmed cancers were detected by either technique, and only 3 out of 177 negative biopsies were misdiagnosed by both techniques as tumors (MRI false positives). Considering that biopsies often suffer from sampling errors, histology of radical prostatectomy specimens is required to confirm that this indeed was misdiagnosis. Perfect sensitivity of the combined DTI and DCE MRI, achieved in this study, strongly suggests that both techniques provide complementary information. It has been shown that low average water diffusivity in the tumors is likely related to high cellular density [25], whereas high K^{trans} is associated with increased microvessel density and leaky vasculature [4]. Since both are expected to be present in the cancer, the combination of DTI and DCE MRI will more likely be able to detect cancer than each technique alone. This is also reflected in the results of the logistic regression modeling, which showed that the model based on all 5 MRI parameters measured in this study performed significantly better than models based on either DTI or DCE MRI parameters alone.

A number of studies have recently shown that various combinations of T_2-weighted MRI, DTI, DCE MRI and MRSI techniques improve sensitivity and specificity of prostate cancer diagnosis [7–14]. The majority of these studies, however, employed a qualitative data analysis with an experienced reader assigning a score reflecting probability of cancer based on the qualitative assessment of the image intensity. In the current study we used a more objective, quantitative approach, where the presence or absence of cancer is evaluated based on the numerical values of 5 MRI parameters calculated from DTI and DCE MRI data. In addition, the logistic regression modeling used in this study, allows constructing a predictor that can estimate the probability of any pixel within parametric maps representing a tumor. Correlation between such predictor maps and histology of whole mount sections should be able to demonstrate whether the combination of the two MRI techniques can accurately estimate the tumor location and volume.

There have only been a few studies that applied a combination of diffusion and DCE MRI techniques in prostate cancer diagnosis [13, 14, 26, 27]. In our earlier study conducted at 1.5T [14], we also showed improved diagnostic capabilities of the combined diffusion and DCE MRI, albeit with lower sensitivities than reported here. We did not carry out concurrent MRI exams at 1.5T and 3.0T, as it would not be possible to ask each patient to go through both a 1.5T and a 3.0T examination. However, considering similar age, PSA and Gleason score distributions within patient populations in both studies, one may speculate that the increased sensitivity in the current study is due to increased SNR resulting from the higher magnetic field. More advanced data processing, including motion correction of both DTI and DCE MRI data, and the use of patient specific AIF, might have also contributed to improved data quality which increased the overall sensitivity of the MRI techniques. However, despite the increased sensitivities of both diffusion and DCE MRI, the combination of the two remains significantly better in diagnosing prostate cancer.

Noworolski et al [26] used the combination of DTI and DCE MRI techniques to distinguish between glandular/ductal and stromal tissues in the prostate gland. They argued that DTI measures diffusion properties of water both in the extracellular space within the stromal tissue and inside the ducts and glands in the glandular/ductal tissue. DCE MRI, however, detects image enhancement in the stromal tissue only, since the contrast agent does not penetrate into the glands and ducts. They suggested that, since higher grade cancers have fewer ducts, a combination of diffusion and DCE MRI may predict the tumor's Gleason score. Our current study does not confirm this hypothesis, as we have found no obvious relationship between the Gleason score and any combination of <D> and K^{trans}. However, the proper correlation between MRI and the Gleason score needs to be carried out based on whole mount histology, which was not done in this study.

There is some controversy in the literature as to whether DTI of the prostate cancer contributes additional information, as compared to more commonly used Diffusion Weighted (DW) MRI techniques. While it has been shown in multiple studies that the average diffusivity (or Apparent Diffusion Coefficient ADC) is significantly lower in the prostatic carcinoma (PCa), as compared to the normal peripheral zone (PZ) [7, 8, 10, 14], the fractional anisotropy (FA) values in the PCa were reported to be higher [28, 29], lower [30], or unchanged [31, 32], comparing to the normal PZ. The average FA values measured in this study generally correspond well to those previously reported [28, 29, 32, 33], however we did not find any differences in FA between PCa, PZ, and CG. Xu et al [31] correlated morphology of the prostate specimens with in vivo and ex vivo DTI measurements of PCa in patients undergoing prostatectomy. They found high diffusion anisotropy in the stromal components within BPH and in the fibrous tissue surrounding the BPH, whereas the anisotropy was not evident in the tissue dominated by epithelial cells, e.g. PCa, normal PZ and epithelial BPH. The low FA values in PZ and PCa, measured in this study, corroborate these results. However, we did not distinguish between BPH and normal central gland in our measurements, thus the low FA values in CG, in our study, likely represent an average of FA values for stromal and epithelial BPH, as well as fibrous tissue in the normal CG.

Fractional volume of the extra-vascular extra-cellular space v_e was lower in PCa as compared to normal PZ, however this difference was not statistically significant ($p = 0.28$). It is somewhat consistent with the average diffusivity <D> being significantly lower in PCa than in normal PZ. The recent work by Gibbs et al., showed statistically significant correlation between Apparent Diffusion Coefficient (ADC) and cell density in prostate cancer [34], thus decreased <D> in tumors is likely resulting from the decreased extra-cellular space. However, v_e does not entirely correspond to the extra-cellular compartment measured with diffusion MRI, but rather represents the contrast agent leakage space. As was suggested by Noworolski et al [35], the ducts in the normal prostate are surrounded by a layer of tightly packed epithelial cells that prevent the contrast agent from crossing into the ducts. However, since the ducts are large, they contribute to the <D> measurements. In tumors this epithelial cell layer is disrupted by the invading cancer cells, making it possible for the contrast agent to enter the ducts. In addition, malignant epithelial cells will spontaneously form glands; however these glands do not have a basal cell layer and thus the contrast agent can cross into the lumen inside these glands. Thus, within the tumor one may expect to see the areas of densely packed cancer cells as well as the areas of disrupted prostatic ducts and malignant glands with the increased contrast agent leakage space. This may explain why differences in v_e between PCa and normal PZ are not as significant as the differences in <D>. However, since for higher grade tumors the amount of malignant gland lumen formation decreases, one may expect that v_e will become more of a measure of the extra-cellular space, and therefore may prove to be useful in characterizing the pathological grade of the tumor.

Fractional plasma volume v_p was significantly smaller in PCa as compared to normal PZ and CG in this study. This result is somewhat surprising, since high contrast enhancement in the tumor is attributed to high microvessel density [20]. The average v_p values in the normal PZ and CG were 1.8% and 1.7% respectively, which represents fairly well the expected fractional volume of the vascular component in the normal prostate. However, the average v_p value of 0.6% in the tumor is likely an order of magnitude too low. This discrepancy may likely be explained by the lower accuracy of fitting the DCE data into the extended Kety model in the fast enhancing regions. This is especially the case when the relatively low temporal resolution of the DCE data prevents accurate sampling of the very fast initial image intensity enhancement, which was likely the case in this study. This is also supported by the fact that in the logistic regression model built on all 5 MRI parameters, v_p did not significantly contribute to the predictor value, thus suggesting that v_p and K^{trans} were not independent parameters of the model.

The ability to detect cancer with close to 100% accuracy has very significant consequences for prostate cancer diagnosis, prognosis and therapy. The fact that the combination “DTI or DCE” is highly sensitive, while the “DTI and DCE” is highly specific, provides additional options in patient management. For example, individuals with elevated PSA, normal digital rectal examination (DRE) and at least one negative biopsy could be followed expectantly with MRI and be reassured that a cancer has not been missed, or alternatively have repeat biopsy of suspicious areas. The ability to fuse MRI with a 3D ultrasound probe would enable highly accurate and minimal number of repeat cores. The high accuracy of 3.0T DTI/DCE MRI provides a particularly suitable method of monitoring, and also guiding

subsequent biopsies should there be a change in clinical parameters (e.g. PSA or DRE). Another potential benefit would involve the use of focal therapy in men with low risk prostate cancer. Also, one may argue that one of the reasons for the use of MRI in non-invasive diagnosis is to limit the number of biopsy procedures. Thus, if MRI can be shown to perform as well as biopsy, this may limit the need for this invasive procedure, especially in men with low risk cancers in an Active Surveillance program or considering focal therapy.

There are several limitations to the current study. Firstly, the number of patients with positive biopsies is rather limited. This was largely because patients in this study were recruited prior to biopsy. Such recruitment process ensures that the study is truly prospective in its assessment as a diagnostic tool, and that no artifacts resulting from biopsies are present in the MRI images. Secondly, the study concentrated on detecting tumors in the peripheral zone. This is partly due to the fact that 70% of prostate tumors are located in the peripheral zone. In addition, only 5% – 10% of patients will have cancer in the transitional zone and no cancer in the peripheral zone. As a result, the standard biopsy protocol does not include the transitional zone. However, in the future studies we will correlate MRI results with histology of whole mount sections, which will test the performance of the combined diffusion and DCE MRI in the transitional zone as well.

In conclusion, our study demonstrated that the combination of the 3T DTI and DCE MRI has significantly better accuracy of prostate cancer diagnosis than either technique alone, with the combination “DTI or DCE” having perfect sensitivity and the combination “DTI and DCE” nearly perfect specificity.

References

1. Sinha S, Sinha U. In vivo diffusion tensor imaging of the human prostate. Magn Reson Med. 2004; 52:530–537. [PubMed: 15334571]
2. Gibbs, P., Pickles, MD., Sreenivas, M., Knowles, A., Turnbull, LW. Diffusion Tensor Imaging of the Normal and Pathologi Prostate at 3T. Proceedings of the 13th Annual Meeting of ISMRM; Miami. 2005. p. 1940
3. Engelbrecht MR, Huisman HJ, Laheij RJ, Jager GJ, van Leenders GJ, Hulsbergen-van de Kaa CA, de la Rosette JJ, Blickman JG, Barentsz JO. Discrimination of prostate cancer from normal peripheral zone and central gland tissue by using dynamic contrast-enhanced MR imaging. Radiology. 2003; 229:248–254. [PubMed: 12944607]
4. Buckley DL, Roberts C, Parker GJ, Logue JP, Hutchinson CE. Prostate cancer: evaluation of vascular characteristics with dynamic contrast-enhanced T1-weighted MR imaging--initial experience. Radiology. 2004; 233:709–715. [PubMed: 15498903]
5. Kurhanewicz J, Vigneron DB, Hricak H, Narayan P, Carroll P, Nelson SJ. Three-dimensional H-1 MR spectroscopic imaging of the in situ human prostate with high (0.24–0.7-cm3) spatial resolution. Radiology. 1996; 198:795–805. [PubMed: 8628874]
6. Parivar F, Hricak H, Shinohara K, Kurhanewicz J, Vigneron DB, Nelson SJ, Carroll P. Detection of locally recurrent prostate cancer after cryosurgery: evaluation by transrectal ultrasound, magnetic resonance imaging, and three-dimensional proton magnetic resonance spectroscopy. Urology. 1996; 48:594–599. [PubMed: 8886066]
7. Reinsberg SA, Payne GS, Riches SF, Ashley S, Brewster JM, Morgan VA, deSouza NM. Combined use of diffusion-weighted MRI and 1H MR spectroscopy to increase accuracy in prostate cancer detection. AJR Am J Roentgenol. 2007; 188:91–98. [PubMed: 17179350]
8. Kajihara H, Hayashida Y, Murakami R, Katahira K, Nishimura R, Hamada Y, Kitani K, Kitaoka M, Suzuki Y, Kitajima M, Hirai T, Morishita S, Awai K, Yamashita Y. Usefulness of Diffusion-

Weighted imaging in the localization of prostate cancer. Int J Radiat Oncol Biol Phys. 2008; 74:399–403. [PubMed: 19019564]

9. Villeirs GM, Oosterlinck W, Vanherreweghe E, De Meerleer GO. A qualitative approach to combined magnetic resonance imaging and spectroscopy in the diagnosis of prostate cancer. Eur J Radiol. 2008 in press.
10. Haider MA, van der Kwast TH, Tanguay J, Evans AJ, Hashmi AT, Lockwood G, Trachtenberg J. Combined T2-weighted and diffusion-weighted MRI for localization of prostate cancer. AJR Am J Roentgenol. 2007; 189:323–328. [PubMed: 17646457]
11. Cheikh AB, Girouin N, Colombel M, Maréchal JM, Gelet A, Bissery A, Rabilloud M, Lyonnet D, Rouvière O. Evaluation of T2-weighted and dynamic contrast-enhanced MRI in localizing prostate cancer before repeat biopsy. Eur Radiol. 2009; 19:770–778. [PubMed: 18925403]
12. Chen M, Dang HD, Wang JY, Zhou C, Li SY, Wang WC, Zhao WF, Yang ZH, Zhong CY, Li GZ. Prostate cancer detection: comparison of T2-weighted imaging, diffusion-weighted imaging, proton magnetic resonance spectroscopic imaging, and the three techniques combined. Acta Radiol. 2008; 49:602–610. [PubMed: 18568549]
13. Langer, DL., van der Kwast, TH., Evans, AJ., Trachtenberg, J., Wilson, BC., Haider, MA. Prostate Cancer Detection: Multi-Parametric MRI with Diffusion Weighted Imaging and Dynamic Contrast Enhanced MRI. Proceedings of the 17th Annual Meeting of ISMR; Honolulu. 2009. p. 782
14. Kozlowski P, Chang SD, Jones EC, Berean KW, Chen H, Goldenberg SL. Combined diffusion-weighted and dynamic contrast-enhanced MRI for prostate cancer diagnosis--correlation with biopsy and histopathology. J Magn Reson Imaging. 2006; 24:108–113. [PubMed: 16767709]
15. Parker GJ, Suckling J, Tanner SF, Padhani AR, Revell PB, Husband JE, Leach MO. Probing tumor microvascularity by measurement, analysis and display of contrast agent uptake kinetics. J Magn Reson Imaging. 1997; 7:564–574. [PubMed: 9170043]
16. Parker GJ, Roberts C, Macdonald A, Buonaccorsi GA, Cheung S, Buckley DL, Jackson A, Watson Y, Davies K, Jayson GC. Experimentally-derived functional form for a population-averaged high-temporal-resolution arterial input function for dynamic contrast-enhanced MRI. Magn Reson Med. 2006; 56:993–1000. [PubMed: 17036301]
17. Meng, R., Maedler, B., Chang, SD., Jones, EC., Goldenberg, SL., Kozlowski, P. 3T DCE MRI in prostate cancer – comparison between population average and patient specific Arterial Input Function. Proceedings of the 17th Annual Meeting of ISMR; Honolulu. 2009. p. 2240
18. Tofts PS, Brix G, Buckley DL, Evelhoch JL, Henderson E, Knopp MV, Larsson HB, Lee TY, Mayr NA, Parker GJ, Port RE, Taylor J, Weisskoff RM. Estimating kinetic parameters from dynamic contrast-enhanced T(1)-weighted MRI of a diffusable tracer: standardized quantities and symbols. J Magn Reson Imaging. 1999; 10:223–232. [PubMed: 10508281]
19. Hosseinzadeh K, Schwarz SD. Endorectal diffusion-weighted imaging in prostate cancer to differentiate malignant and benign peripheral zone tissue. J Magn Reson Imaging. 2004; 20:654–661. [PubMed: 15390142]
20. Padhani AR, Gapinski CJ, Macvicar DA, Parker GJ, Suckling J, Revell PB, Leach MO, Dearnaley DP, Husband JE. Dynamic contrast enhanced MRI of prostate cancer: correlation with morphology and tumour stage, histological grade and PSA. Clin Radiol. 2000; 55:99–109. [PubMed: 10657154]
21. Mould, RF. Introductory Medical Statistics. 3. Bristol and Philadelphia: Institute of Physics Publishing; 1998. Sensitivity and Specificity; p. 232-233.
22. Newcombe RG. Two-sided confidence intervals for the single proportion: comparison of seven methods. Stat Med. 2008; 17:857–872.
23. Berkson J. Application of the logistic function to bio-assay. J Am Stat Assoc. 1944; 39:357–365.
24. DeLong ER, DeLong DM, Clarke-Pearson DL. Comparing the areas under two ormore correlated Receiver Operating Characteristics curves: A nonparametric approach. Biometrics. 1988; 44:837–845. [PubMed: 3203132]
25. Lyng H, Haraldseth O, Rofstad EK. Measurement of cell density and necrotic fraction in human melanoma xenografts by diffusion weighted magnetic resonance imaging. Magn Reson Med. 2000; 43:828–836. [PubMed: 10861877]

26. Noworolski SM, Vigneron DB, Chen AP, Kurhanewicz J. Dynamic contrast-enhanced MRI and MR diffusion imaging to distinguish between glandular and stromal prostatic tissues. Magn Reson Imaging. 2008; 26:1071–1080. [PubMed: 18508221]
27. Yoshizako T, Wada A, Hayashi T, Uchida K, Sumura M, Uchida N, Kitagaki H, Igawa M. Usefulness of diffusion-weighted imaging and dynamic contrast-enhanced magnetic resonance imaging in the diagnosis of prostate transition-zone cancer. Acta Radiol. 2008; 49:1207–1213. [PubMed: 19031184]
28. Gibbs P, Pickles MD, Turnbull LW. Diffusion imaging of the prostate at 3.0 tesla. Invest Radiol. 2006; 41:185–188. [PubMed: 16428991]
29. Gürses B, Kabakci N, Kovanlikaya A, Firat Z, Bayram A, Ulug AM, Kovanlikaya I. Diffusion tensor imaging of the normal prostate at 3 Tesla. Eur Radiol. 2008; 18:716–721. [PubMed: 17960389]
30. Manenti G, Carlani M, Mancino S, Colangelo V, Di Roma M, Squillaci E, Simonetti G. Diffusion tensor magnetic resonance imaging of prostate cancer. Invest Radiol. 2007; 42:412–419. [PubMed: 17507813]
31. Xu J, Humphrey PA, Kibel AS, Snyder AZ, Narra VR, Ackerman JJ, Song SK. Magnetic resonance diffusion characteristics of histologically defined prostate cancer in humans. Magn Reson Med. 2009; 61:842–850. [PubMed: 19215051]
32. Takayama Y, Kishimoto R, Hanaoka S, Nonaka H, Kandatsu S, Tsuji H, Tsujii H, Ikehira H, Obata T. ADC value and diffusion tensor imaging of prostate cancer: changes in carbon-ion radiotherapy. J Magn Reson Imaging. 2008; 27:1331–1335. [PubMed: 18504751]
33. Gibbs P, Pickles MD, Turnbull LW. Repeatability of echo-planar-based diffusion measurements of the human prostate at 3 T. Magn Reson Imaging. 2007; 25:1423–1429. [PubMed: 17499468]
34. Gibbs P, Liney GP, Pickles MD, Zelhof B, Rodrigues G, Turnbull LW. Correlation of ADC and T2 measurements with cell density in prostate cancer at 3.0 Tesla. Invest Radiol. 2009; 44:572–576. [PubMed: 19692841]
35. Noworolski, SM., Chen, AP., Vigneron, DB., Kurhanewicz, J. Assessment of prostatic ductal volume using combined Dynamic Contrast-Enhanced MRI and Diffusion MRI. Proceedings of the 11th Annual Meeting of ISMRM; Toronto. 2003. p. 1464

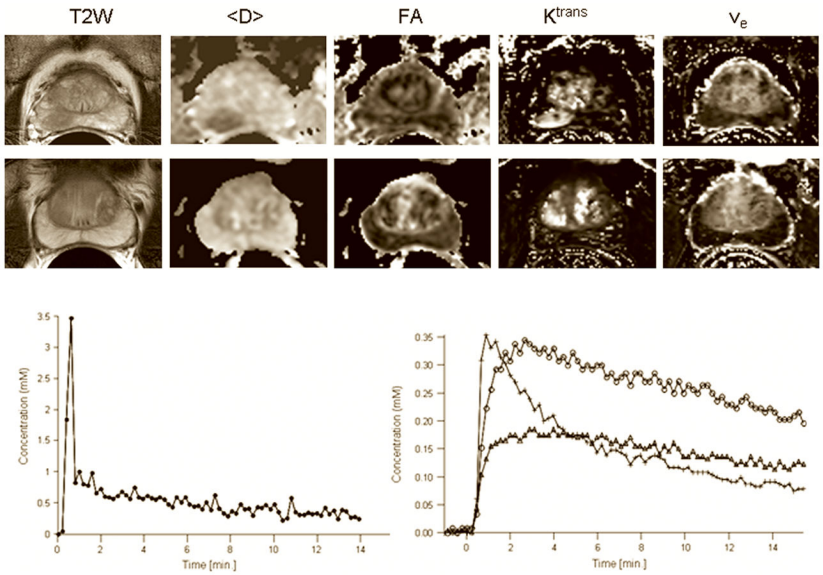

Figure 1.

Figure 1a. T_2 weighted images and the corresponding <D>, FA, K^{trans} and v_e maps from a 67 years old patient with PSA = 7.1 ng/mL, who had biopsy proven adenocarcinoma in the right midgland (top) and negative biopsies in another patient (69 years old, PSA = 4.6 ng/mL) (bottom). The tumor in the right midgland of the peripheral zone is clearly visible as a hypointense area on the T_2 weighted image and <D> map, and as a hyperintense area on the K^{trans} map (top row). Note that neither FA nor v_e show differences between the tumor and the normal peripheral zone, which is consistent with the average values of these parameters across the patient population in this study (see Table 2). Although K^{trans} values in some areas of the central gland appear as high as in the tumor, the average K^{trans} value across the patient population in the tumor was significantly higher than in the central gland.

Figure 1b. AIF (left) and representative concentration vs. time curves (right) from PCa (crosses), normal PZ (open triangles) and CG (open circles) extracted from the DCE data shown at the top of Figure 1a. Zero on the time axis corresponds to the bolus arrival time in the external femoral artery. Note that the concentration vs. time curves were adjusted for the bolus arrival time.

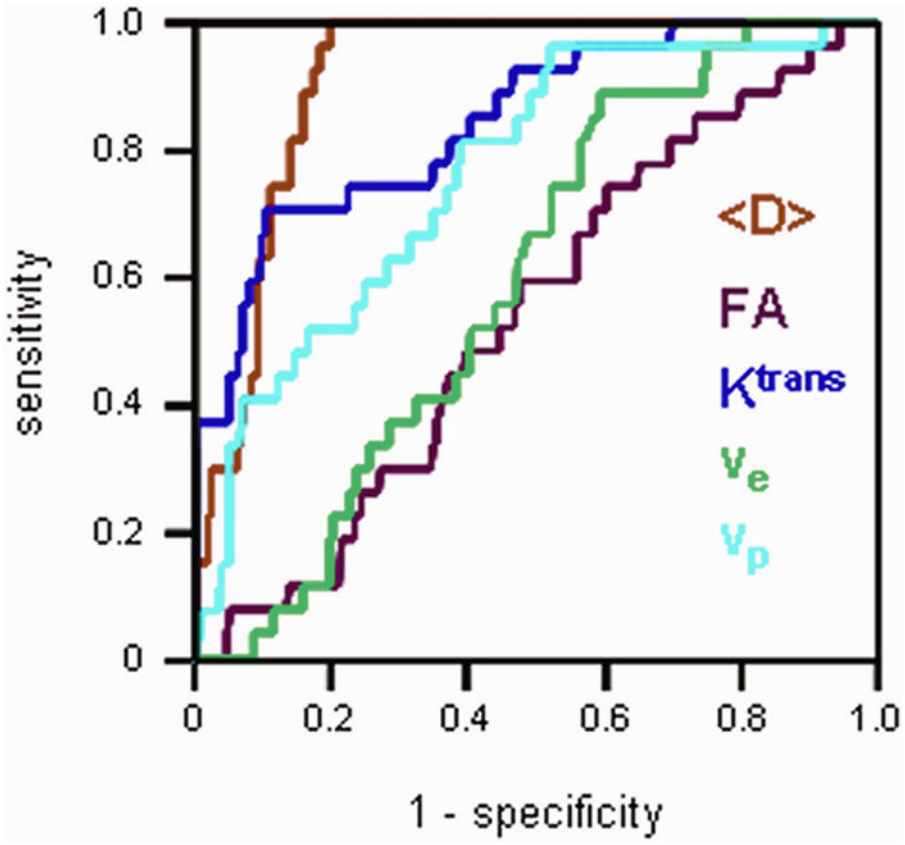

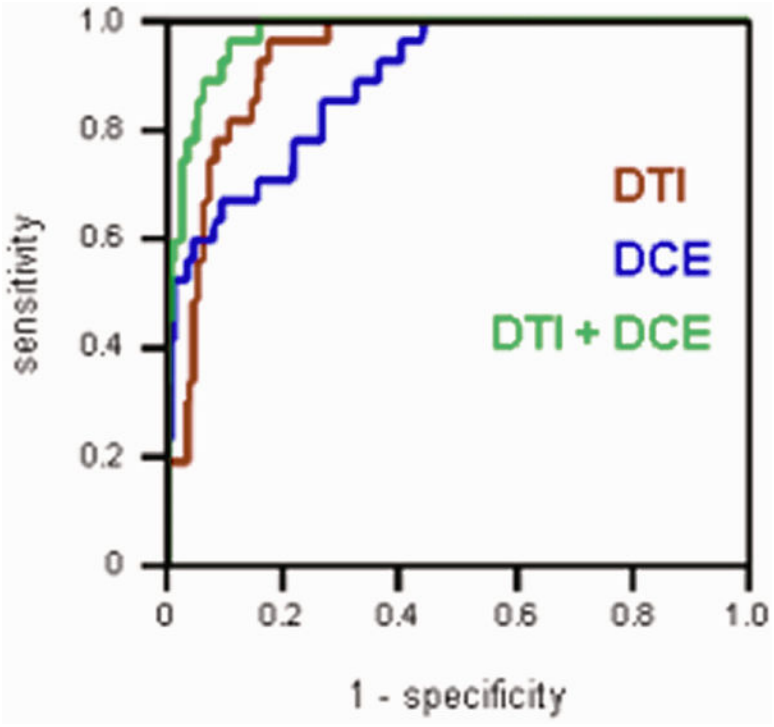

Figure 2.

Figure 2a. ROC curves generated for each MRI parameter. The average diffusivity <D>had the largest area under the ROC curve. ROC curves for the FA and v_e lay close to the diagonal, suggesting that these parameters alone are not particularly useful in distinguishing between cancer and normal PZ.

Figure 2b. ROC curves generated with the logistic regression model for: DTI parameters (red), DCE MRI parameters (blue), and DTI + DCE MRI parameters (green). The AUC calculated for DTI + DCE MRI parameters was significantly higher than that for either the DTI or the DCE MRI parameters alone.

Table 1

Clinical data for 10 patients with biopsy confirmed cancer.

Patient	age [years]	PSA [ng/mL]	number of positive biopsies	biopsy Gleason score	prostatectomy Gleason score	clinical stage
P003	62	5.3	5	3+4	4+3	cT2a
P004	67	7.1	4	3+4	3+4	cT2b
P005	60	5.4	2	3+3	n/a	n/a
P007	58	7.1	5	4+5	3+4	cT1c
P010	55	7.09	2	3+3	n/a	cT1c
P015	72	12	3	4+4, 4+5	4+5	cT1c
P016	65	5.43	2	4+3, 3+3	3+4	cT1c
P020	64	6.8	2	3+4	3+4	cT2a
P024	60	5.4	1	4+4	4+3	cT1c
P026	62	6.4	1	3+3	n/a	cT2a

Table 2

Average values (mean ± standard deviation) of DTI and DCE MRI parameters.

	<D> [10^{-3}mm^2/sec]	FA	K^{trans} [min^{-1}]	v_e	v_p
PCa	1.07 ± 0.12[a,b]	0.20 ± 0.05	0.18 ± 0.06[a,b]	0.20 ± 0.05[c]	0.006 ± 0.008[a,b]
PZ	1.76 ± 0.23[b]	0.20 ± 0.06	0.06 ± 0.03[b]	0.24 ± 0.13[c]	0.018 ± 0.012
CG	1.61 ± 0.12	0.20 ± 0.03	0.11 ± 0.04	0.29 ± 0.11	0.017 ± 0.009

[a] – significantly different than PZ ($p<0.001$)

[b] – significantly different than CG ($p<0.001$)

[c] – significantly different than CG ($p<0.01$)

<D> – mean diffusivity, FA – fractional anisotropy

K^{trans} – volume transfer constant, v_e – fractional volume of the extra-vascular extra-cellular space, v_p – fractional plasma volume

PCa – prostatic adenocarcinoma (DTI: n = 25, DCE MRI: n = 19), PZ – normal peripheral zone (DTI: n = 147, DCE MRI: n = 133), CG – central gland (DTI: n = 40, DCE MRI: n = 40)

Table 3

Performance measures for the DTI and DCE MRI and their combinations.

	DTI	DCE MRI	DTI and DCE MRI	DTI or DCE MRI
sensitivity	81% (22/27) (74% – 87%)	63% (17/27) (55% – 70%)	44% (12/27) (37% – 52%)	100% (27/27) (97% – 100%)
specificity	85% (167/196) (79% – 90%)	90% (160/177) (85% – 94%)	98% (174/177) (94% – 100%)	77% (136/177) (69% – 83%)
PPV	43% (22/51) (35% – 51%)	50% (17/34) (42% – 58%)	80% (12/15) (73% – 86%)	40% (27/68) (32% – 48%)
NPV	97% (167/172) (93% – 94%)	94% (160/170) (89% – 97%)	93% (174/187) (88% – 96%)	100% (136/136) (97% – 100%)
accuracy	85% (189/223) (78% – 90%)	87% (177/204) (80% – 91%)	91% (186/204) (85% – 95%)	80% (163/204) (73% – 85%)

DTI – diffusion tensor imaging

DCE MRI – dynamic contrast enhanced MRI

PPV – positive predictive value

NPV – negative predictive value

95% confidence intervals are provided in brackets